# Supplementary Materials for

## Dynamic ventilation functional MRI of the lung with sub-millimeter spatial resolution and millisecond temporal resolution

Hongchuang Li[a,b,1], Haidong Li[a,b,1], Li Fan[c,1] Ming Zhang[a,b], Xiaoling Liu[a,b], Xiuchao Zhao[a,b], Yeqing Han[a,b], Yang Jin[e], Louis-S. Bouchard[f], Shiyuan Liu[c], Xin Zhou[a,b,d,*]

[a] *State Key Laboratory of Magnetic Resonance Spectroscopy and Imaging, National Center for Magnetic Resonance in Wuhan, Wuhan Institute of Physics and Mathematics, Innovation Academy for Precision Measurement Science and Technology, Chinese Academy of Sciences, Wuhan 430071, China*
[b] *University of Chinese Academy of Sciences, Beijing 100049, China*
[c] *Department of Radiology, Second Affiliated Hospital of Naval Medical University, Shanghai 200003, China*
[d] *Key Laboratory of Biomedical Engineering of Hainan Province, School of Biomedical Engineering, Hainan University, Haikou 570228, China*
[e] *Department of Respiratory and Critical Care Medicine, Union Hospital of Tongji Medical College, Huazhong University of Science and Technology, Wuhan 430022, China*
[f] *Departments of Chemistry and Biochemistry, University of California, Los Angeles, CA 90095, USA*
*Corresponding author.

Email: xinzhou@wipm.ac.cn (X. Z.)

[1]These authors contributed equally to this work

**This PDF file includes:**

## 1. Methods and Materials

### *1.1 $^{129}$Xe Polarization and Delivery*

Isotopically enriched xenon gas (86% $^{129}$Xe) was polarized via spin-exchange optical pumping using a commercial polarizer system (verImagin Healthcare; Wuhan, China). The HP $^{129}$Xe gas was cryogenically accumulated and subsequently thawed into a Tedlar bag prior to the MRI experiments. The available spin polarization was approximately 40%. For the MRI experiments, a home-built MR-compatible HP gas delivery system was used, controlled by LabVIEW programs [1]. The inspiration and expiration time for xenon gas were 700 and 1400 ms, respectively, with a tidal volume of 2.5 ml. For oxygen gas, the inspiration and expiration times were 400 ms and 800 ms, respectively, with the same tidal volume. Throughout the examinations, airway pressure was monitored and displayed in real time, and the airway pressure was less than 15 cm$H_2O$.

### *1.2 Animal Preparation*

All animal protocols were approved by the institutional animal care and use committee. Ten male Sprague–Dawley rats (weight, 200 ± 20 g) were randomly assigned to two groups. The five rats in the diseased group received an intratracheal instillation of 0.2 mL LPS solution (3 mg/kg body weight). The remaining five were administered an equivalent volume (0.2 ml) of normal saline as the control group. MRI acquisitions were performed two weeks after the instillation. In addition, another three rats were used to optimize the acquisition parameters for accelerated dynamic MRI. Prior to MRI examinations, each rat was anesthetized and intubated with a 14-guage endotracheal tube following tracheotomy. During imaging, the rat was ventilated in the supine position using the home-built ventilator.

### *1.3 Dynamic MRI Acquisition*

All MRI experiments were conducted on a 7.0 T animal MRI scanner (BioSpec 70/20 USR; Bruker, Ettlingen, Germany) equipped with a high-performance gradient coil (maximum amplitude: ~370 mT/m; maximum slew rate: ~3000 T/m/s) and a home-built birdcage coil with an inner diameter of 55 mm. Rats were ventilated alternatively with xenon and oxygen gases (Fig. 1a). A two-dimensional FLASH with centric phase encoding was used for the MRI acquisition. For the fully sampled (FS) MRI experiments, the following parameters were used: number of frames = 344, TR/TE = 5.6/1.7 ms, flip angle = 7°, matrix = 96 × 96, FOV = 45 mm × 45 mm, bandwidth = 50 kHz, and slice thickness = 35 mm. The total acquisition time was approximately 5 min, and 240 mL of HP xenon gas was used for each examination.

Accelerated HP $^{129}$Xe dynamic MRI with CS was performed in both the LPS-treated ($n$ = 5) and control groups ($n$ = 5). All scan parameters for the accelerated MRI acquisition were identical to those in the FS MRI experiments except for the acceleration factor of 2, resulting in 48 sampled phase encoding steps. The total acquisition time was approximately 2.5 min, and 120 mL of HP xenon gas was used for each examination.

The optimal acquisition patterns were determined using the following steps [2-4]: First, a series of variable-density sampling patterns with acceleration factors ranging from two to four were randomly generated using the Monte-Carlo method. These patterns were then applied to sample the FS k-space data, and the mean absolute error (MAE) between the reconstructed images and FS datasets were calculated. Finally, the acquisition pattern with minimum MAE was selected as the optimal pattern. Considering both image quality and detail, the sampling pattern with an acceleration factor of 2 was chosen.

### *1.4 Data Processing*

All MR data were processed using MATLAB software (MathWorks, Inc., Natick, MA). For the FS dataset, images were normalized by dividing the maximum signal of all the voxel prior MAE and SSIM analysis. For CS datasets of the ten rats, dynamic ventilation images were segmented using a SNR threshold of > 3, as described in previous studies [5,6].

To quantify regional dynamic ventilation function, four ROIs in main trachea (ROI-T), left lobe (ROI-L), right upper lobe (ROI-RU), and right lower lobe (ROI-RL) were manually delineated based on the middle frame, i.e., 150$^{th}$ frame, as shown in Fig. 2a. Prior to further analysis, the images were normalized to the mean signal within the trachea for each rat. Signal–time curves for each ROIs were subsequently generated.

To further extract physiological information from the signal–time curves, all dynamic ventilation images were registered to the 150$^{th}$ frame using rigid registration [7-9]. Signal decay was then corrected for RF pulse excitations. Characteristic time values and airflow rate parameters were defined and calculated on a voxel-by-voxel basis for each rat. The group averaged values of these parameters for each ROI were subsequently calculated [10-12], along with the standard deviation and coefficient of variation (CV) for each ROI.

### *1.5 Statistical Analysis*

Statistical analyses were performed using SPSS software (version 25.0, IBM Inc., Chicago, IL, USA). Data normality was assessed with the Shapiro–Wilk test prior to further analysis. A power analysis was conducted to determine the adequacy of the sample size. Depending on normality assumptions, unpaired two-tailed t-tests were employed for normally distributed variables, while the Mann–Whitney U test was used for non-normally distributed variables. These statistical tests compared the $T_{arrival}$, $T_{peak}$, $Flow_{in}$, and $Flow_{out}$ parameters between the LPS-treated and control groups. In addition, Bonferroni corrections were applied to control type I error rates. Pearson correlation was performed to evaluate the relationship between $^{129}$Xe MRI-derived parameters and histological measurements. A two–tailed *P* value of 0.05 was considered statistically significant for all analyses.

### 1.6 *Histology*

After MRI experiments, the lungs were extracted and inflated with 4% paraformaldehyde solution at an airway pressure of 25 cm $H_2O$ for at least 2 h, followed by storage in the same solution for more than 48 h. The lungs were then embedded in paraffin, sectioned into 5-μm-thick slices, and stained with hematoxylin and eosin. All sections were examined and imaged using a microscope (Eclipse Ts 100; Nikon Corporation, Tokyo, Japan). For each rat, the alveolar septal thickness was measured using Image-Pro Plus software (Media Cybernetics, Buckinghamshire, UK). Histological results from representative LPS-treated and control rats are presented in Fig. S4. Compared with the control group, the alveolar septal thickness increased significantly in the LPS group ($P$ <0.001).

### *1.7 Theoretical Calculation.*

Before further analysis, the measured $^{129}$Xe signal for each voxel was calibrated. As $^{129}$Xe signal acquisition occurs during the breathing cycle, the measured signal is influenced by RF pulse excitations, longitudinal relaxation ( $T_1$) with the lung, and variations in the concentration of HP $^{129}$Xe gas. Accordingly, the measured $^{129}$Xe signal from a given voxel ($i$) after the application of the $j^{th}$ RF pulse can be expressed as:

$$S_{i,j} = S_{i,j-1} exp(-TR/T_1) \cdot cos\,\theta + S_{i,\,variation}(j)\,, \tag{S1}$$

where $S_{i,j}$ and $S_{i,j-1}$ denote the $^{129}$Xe signals within the $i^{th}$ voxel after the application of the $j^{th}$ and $(j\text{-}1)^{th}$ RF pulses, respectively. $S_{i,variation}$ represents the variation in the HP gas signal between these two RF

pulses and $\theta$ denotes the flip angle. Given that the typical value of $T_1$ (~10 s) is much longer than the interval between the $j^{th}$ and $(j\text{-}1)^{th}$ acquisition (5.6 ms), the effects of $T_1$ relaxation in the lungs can be neglected. Therefore, the equation (S1) can be rewritten as:

$$S_{i,variation}(j) = S_{i,j} - S_{i,j-1} \cdot \cos\theta \tag{S2}$$

As MR data were acquired during the respiratory process, HP $^{129}$Xe gas continuously flows into/out of the voxel. Consequently, the measured $^{129}$Xe signal intensity is also influenced by RF pulse excitations that occur before the gas arrives at the voxel. Therefore, equation (S2) must be modified as

$$S_{i,variation}(j) = \left(S_{i,j} - S_{i,j-1} \cdot \cos\theta\right) / (\cos\theta)^{(T_{arrival}(i))/TR} \tag{S3}$$

where $T_{arrival}(i)$ represents the time-of-flight of the gas from the trachea to the voxel $i$. At time $\tau$, the total HP $^{129}$Xe gas signal $S_{i,total}(\tau)$ detected in this voxel can be calculated by summing all $S_{i,variation}$ values over the time period $\tau$:

$$S_{i,total}(\tau) = \sum_{j=1}^{\tau/TR} S_{i,variation}(j) \tag{S4}$$

The total HP $^{129}$Xe gas signal detected across the WL, $S_{wl,total}(\tau)$, can be calculated using the same method, i.e., replacing the voxel signal $S_{i,j}$ with the WL signal $S_{whole\ lung,\ j}$. Subsequently, the total HP xenon gas volume $V_{i,total}$ within the voxel $i$ can be calculated using the following equation:

$$V_{i,total}(\tau) = S_{i,total}(\tau) / (C \cdot f \cdot P) \tag{S5}$$

where $f$ is a constant, determined by the experimental setup; $P$ is the $^{129}$Xe polarization level; and $C$ is the $^{129}$Xe gas concentration per unit volume under room temperature and pressure. Given that the tidal volume for HP xenon gas is known ($V_{tidal}=2.5\ mL$), the relationship between the tidal volume and the xenon gas signal can be expressed as

$$V_{tidal} = S_{wl,\ total}(\tau_{max}) / (C \cdot f \cdot P) \tag{S6}$$

where $\tau_{max}$ is the time at which $S_{wl,total}(\tau)$ reaches its maximum. Therefore, equation (S5) can be rewritten as

$$V_{i,total}(\tau) = S_{i,total}(\tau) \cdot V_{tidal} / S_{wl,\ total}(\tau_{max}) \tag{S7}$$

Then, HP xenon gas volume–time curve for each voxel can be obtained (as shown in Fig. 2h), exhibiting good linearity during inspiration and expiration phases. Therefore, the gas flow rate during inspiration ($Flow_{in}(i)$) and the total HP gas volume $V_{i,total}(\tau)$ in the voxel *i* can be expressed as

$$V_{i,\,total}(\tau)=Flow_{in}(i)\cdot\tau,\ T_{arrival}\le\tau\le T_{peak}*0.95 \tag{S8}$$

To minimize interference from the non-linear portion near the peak signal, two empirical thresholds of $T_{peak}*0.95$ and $T_{peak}*1.05$ were applied to select the fitting interval. Similarly, the gas flow rate during expiration ($Flow_{out}$) of the lung could also be calculated using the same method.

## 2. Figures and Tables

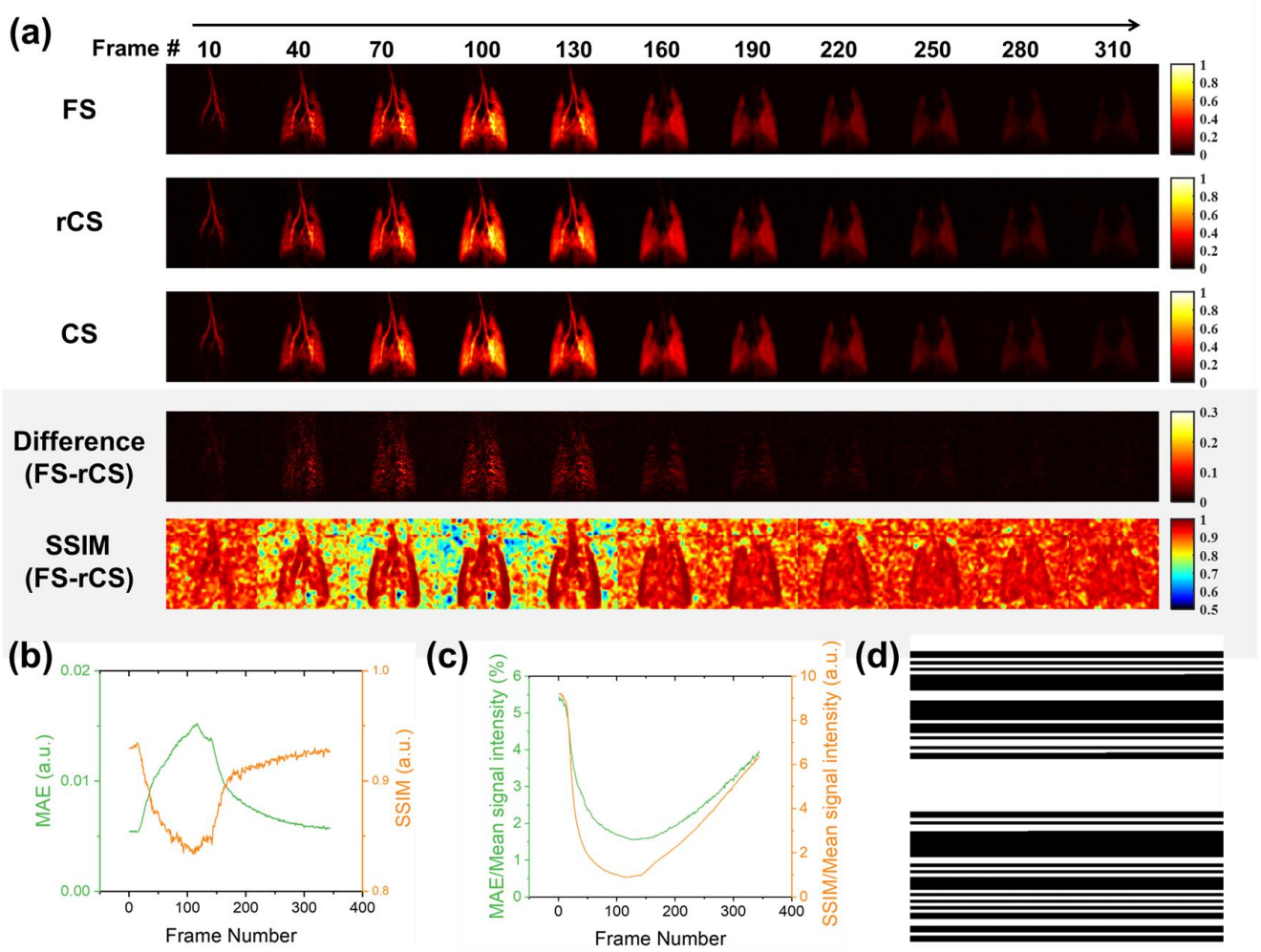


**Fig. S1.** Fidelity assessment of dynamic ventilation images obtained using compressed sensing. (a) Representative frames of dynamic ventilation images acquired with fully sampled (FS), retrospective compressed sensing (rCS), and prospective compressed sensing (CS) techniques. Corresponding difference maps and structural similarity index (SSIM) maps calculated by comparing rCS to FS images are also presented. (b) Plots of MAE/mean signal intensity and SSIM/mean signal intensity (c) various with frames. Retrospective and prospective results demonstrate that the quality of the dynamic images captured using the adopted acquisition strategy was comparable to that achieved with the fully sampled acquisition strategy. The measured SSIM and mean MAE across all frames for the retrospective CS and FS strategies were 0.89 ± 0.03 and 0.009 ± 0.003, respectively. (d) Undersampling patterns used for rCS and CS acquisitions.

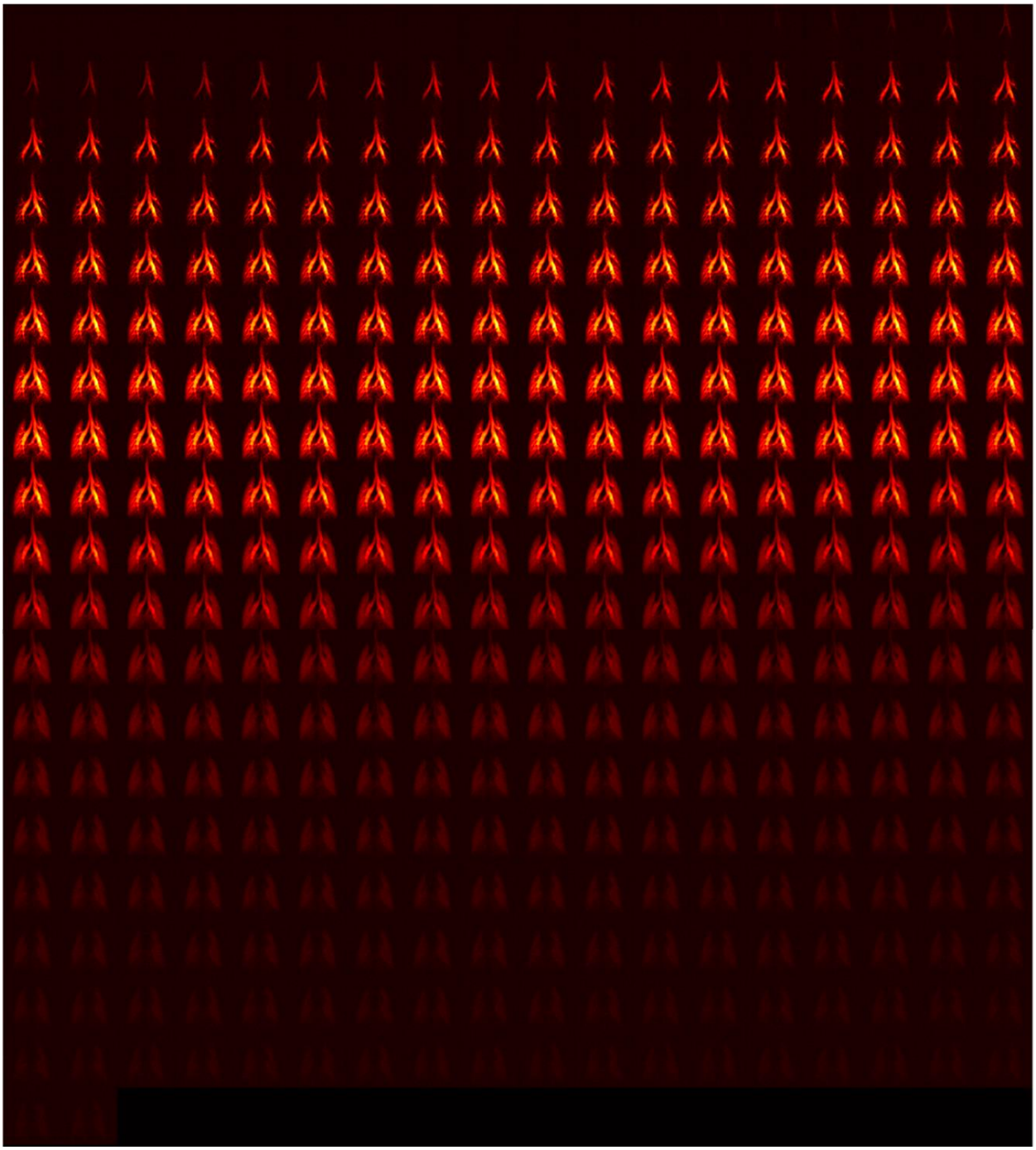

**Fig. S2.** Representative dynamic images acquired throughout the entire respiratory cycle.

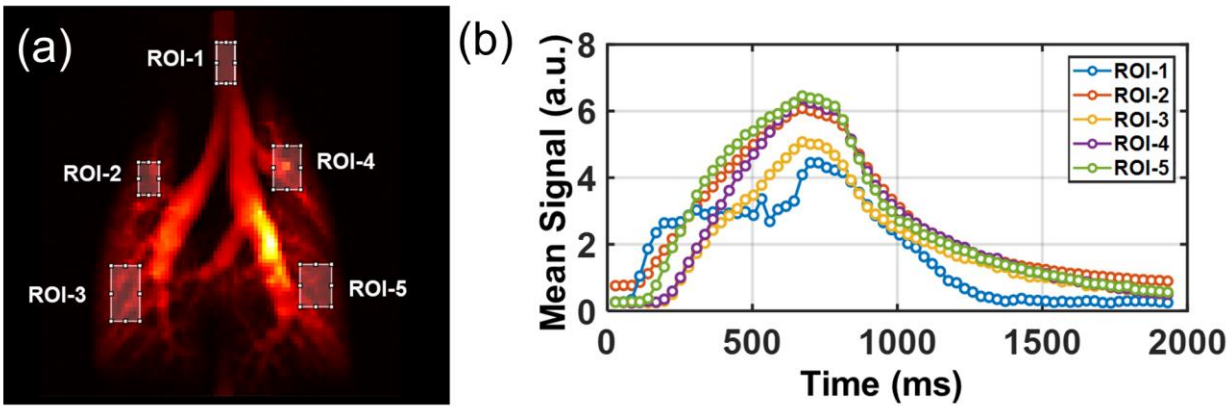


**Fig. S3.** Five typical ROIs selected for dynamic ventilation analysis (a) and their corresponding signal changes over time throughout the whole respiratory cycle (b). All images were normalized to the average signal intensity of all frames.

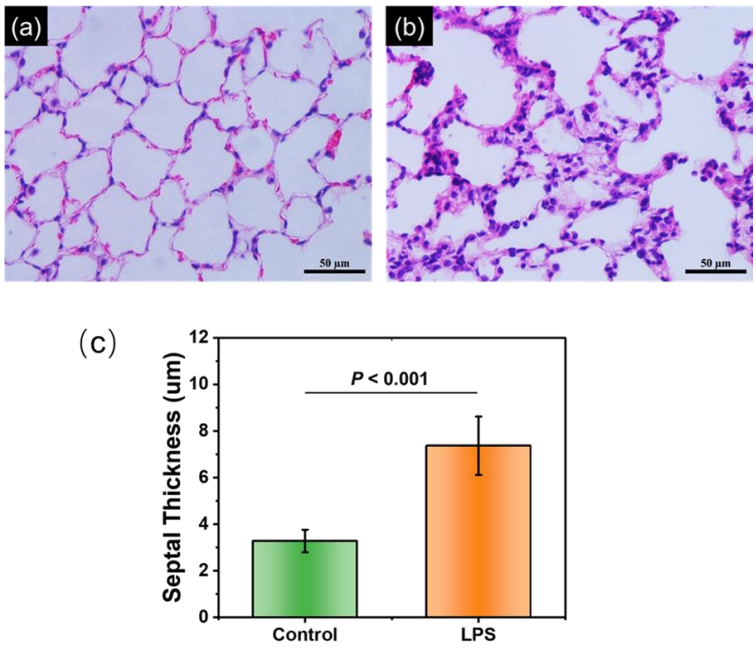


**Fig. S4.** Representative H&E-stained lung images. (a) Control rat and (b) LPS-treated rat. Notably, thickening of the alveolar septa is observed in the LPS-treated rat. Scale bar: 50 μm. (c) Comparison of septal thickness between the two groups as measured from histology. A significant increase was observed in the LPS group ($P$ <.001)

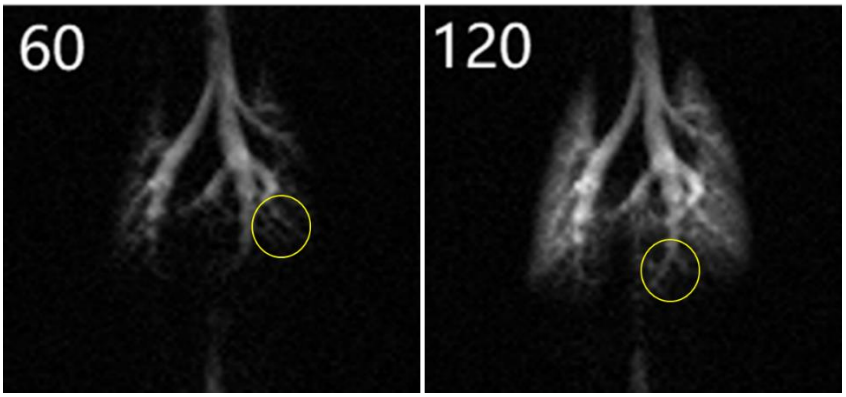


**Fig. S5.** Visualization of the small airways using the proposed method

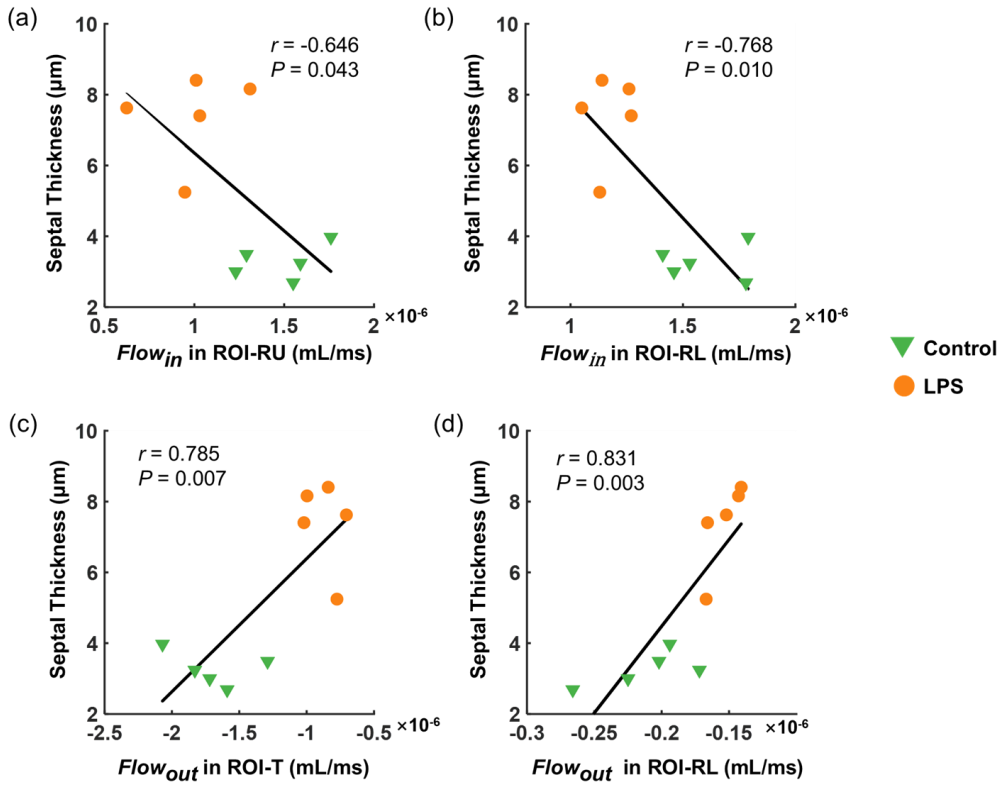


**Fig. S6.** Correlations between MRI - derived ventilation metrics ($Flow_{in}$ and $Flow_{out}$) and histological measurements of septal thickness.

**Table S1.** Averaged $T_{arrival}$ and $T_{peak}$ values for all the ROIs derived from dynamic ventilation images for each rat.

| | | | WL | ROI-T | ROI-LL | ROI-RU | ROI-RL |
|---|---|---|---|---|---|---|---|
| $T_{arrival}$ (ms) | Control Rats | 1 | 167 ± 84 | 68 ± 14 | 145 ± 50 | 125 ± 31 | 142 ± 46 |
| | | 2 | 164 ± 81 | 67 ± 10 | 153 ± 55 | 119 ± 30 | 149 ± 52 |
| | | 3 | 181 ± 87 | 68 ± 9 | 162 ± 53 | 155 ± 48 | 193 ± 72 |
| | | 4 | 173 ± 89 | 64 ± 10 | 165 ± 54 | 128 ± 34 | 161 ± 65 |
| | | 5 | 159 ± 77 | 71 ± 9 | 162 ± 48 | 120 ± 31 | 138 ± 45 |
| | | Mean ± SD | 169 ± 8 | 68 ± 2 | 157 ± 7 | 130 ± 13 | 157 ± 20 |
| | LPS Rats | 1 | 166 ± 73 | 72 ± 15 | 163 ± 47 | 118 ± 26 | 147 ± 42 |
| | | 2 | 174 ± 87 | 60 ± 25 | 168 ± 62 | 126 ± 41 | 156 ± 64 |
| | | 3 | 167 ± 88 | 72 ± 14 | 176 ± 58 | 176 ± 88 | 155 ± 42 |
| | | 4 | 158 ± 73 | 64 ± 10 | 145 ± 46 | 143 ± 47 | 149 ± 59 |
| | | 5 | 156 ± 81 | 58 ± 19 | 148 ± 47 | 129 ± 52 | 147 ± 52 |
| | | Mean ± SD | 164 ± 7 | 65 ± 6 | 160 ± 12 | 139 ± 21 | 150 ± 4 |
| | | *P* | 1.000 | 1.000 | 1.000 | 1.000 | 1.000 |
| $T_{peak}$ (ms) | Control Rats | 1 | 788 ± 148 | 718 ± 70 | 747 ± 79 | 757 ± 54 | 735 ± 67 |
| | | 2 | 795 ± 158 | 735 ± 94 | 770 ± 75 | 757 ± 92 | 746 ± 69 |
| | | 3 | 776 ± 131 | 694 ± 88 | 753 ± 78 | 763 ± 90 | 755 ± 88 |
| | | 4 | 796 ± 146 | 743 ± 51 | 757 ± 70 | 769 ± 101 | 750 ± 63 |
| | | 5 | 801 ± 173 | 735 ± 86 | 796 ± 93 | 743 ± 96 | 763 ± 104 |
| | | Mean ± SD | 791 ± 9 | 725 ± 18 | 765 ± 17 | 758 ± 8 | 750 ± 9 |
| | LPS Rats | 1 | 786 ± 128 | 666 ± 119 | 768 ± 78 | 737 ± 69 | 757 ± 76 |
| | | 2 | 804 ± 161 | 715 ± 134 | 776 ± 78 | 778 ± 120 | 770 ± 95 |
| | | 3 | 764 ± 146 | 758 ± 45 | 738 ± 78 | 802 ± 154 | 754 ± 58 |
| | | 4 | 797 ± 152 | 733 ± 58 | 753 ± 68 | 809 ± 171 | 755 ± 60 |
| | | 5 | 765 ± 136 | 724 ± 87 | 741 ± 55 | 761 ± 151 | 754 ± 90 |
| | | Mean ± SD | 783 ± 16 | 719 ± 30 | 755 ± 15 | 777 ± 26 | 758 ± 6 |
| | | *P* | 1.000 | 1.000 | 1.000 | 0.950 | 0.900 |

Abbreviation: WL, whole lung; ROI-T, ROI-main trachea; ROI-L, ROI-left lobe; ROI-RU, ROI-right upper lobe; ROI-RL, ROI-right lower lobe.

**Table S2.** Airflow rate parameters derived from dynamic ventilation images.

| | | | WL | ROI-T | ROI-LL | ROI-RU | ROI-RL |
|---|---|---|---|---|---|---|---|
| $Flow_{in}$ (×10$^{-6}$ mL/ms) | Control Rats | 1 | 1.14 ± 1.13 | 2.43 ± 1.51 | 1.28 ± 0.86 | 1.29 ± 0.55 | 1.41 ± 1.15 |
| | | 2 | 1.49 ± 1.26 | 2.34 ± 1.46 | 1.66 ± 0.99 | 1.76 ± 0.8 | 1.79 ± 1.28 |
| | | 3 | 1.22 ± 1.24 | 2.4 ± 1.17 | 1.23 ± 0.74 | 1.23 ± 0.73 | 1.46 ± 1.5 |
| | | 4 | 1.49 ± 1.53 | 3.06 ± 1.39 | 1.6 ± 1.17 | 1.55 ± 0.79 | 1.78 ± 1.6 |
| | | 5 | 1.23 ± 0.99 | 2.18 ± 1.15 | 1.26 ± 0.66 | 1.59 ± 0.74 | 1.53 ± 1.06 |
| | | Mean ± SD | 1.31 ± 0.15 | 2.48 ± 0.3 | 1.41 ± 0.18 | 1.48 ± 0.2 | 1.6 ± 0.16 |
| | LPS Rats | 1 | 1.01 ± 1.12 | 2.02 ± 1.24 | 0.84 ± 0.62 | 1.31 ± 0.66 | 1.26 ± 1.34 |
| | | 2 | 0.99 ± 1.33 | 2.01 ± 1.3 | 0.91 ± 0.88 | 0.95 ± 0.96 | 1.13 ± 1.5 |
| | | 3 | 1.14 ± 1.21 | 2.17 ± 0.94 | 1.01 ± 0.69 | 0.62 ± 0.45 | 1.05 ± 0.67 |
| | | 4 | 1.4 ± 1.56 | 2.89 ± 1.5 | 1.3 ± 0.97 | 1.01 ± 0.65 | 1.14 ± 0.73 |
| | | 5 | 1.14 ± 1.22 | 1.96 ± 1.19 | 1.2 ± 0.85 | 1.03 ± 0.67 | 1.27 ± 1.44 |
| | | Mean ± SD | 1.13 ± 0.15 | 2.21 ± 0.35 | 1.05 ± 0.17 | 0.99 ± 0.22 | 1.17 ± 0.08 |
| | | P | 0.62 | 0.475 | 0.115 | 0.045 | 0.010 |
| $Flow_{out}$ (×10$^{-6}$ mL/ms) | Control Rats | 1 | -0.31 ± 0.71 | -1.29 ± 0.75 | -0.18 ± 0.54 | -0.13 ± 0.05 | -0.2 ± 0.69 |
| | | 2 | -0.37 ± 0.87 | -2.07 ± 1.35 | -0.17 ± 0.32 | -0.16 ± 0.07 | -0.19 ± 0.29 |
| | | 3 | -0.49 ± 1.12 | -1.72 ± 0.96 | -0.22 ± 0.36 | -0.24 ± 0.34 | -0.23 ± 0.47 |
| | | 4 | -0.42 ± 0.73 | -1.59 ± 0.68 | -0.23 ± 0.15 | -0.17 ± 0.1 | -0.27 ± 0.22 |
| | | 5 | -0.37 ± 0.71 | -1.83 ± 0.94 | -0.17 ± 0.13 | -0.17 ± 0.3 | -0.17 ± 0.34 |
| | | Mean ± SD | -0.39 ± 0.06 | -1.7 ± 0.26 | -0.19 ± 0.02 | -0.17 ± 0.03 | -0.21 ± 0.03 |
| | LPS Rats | 1 | -0.27 ± 0.47 | -1 ± 0.53 | -0.14 ± 0.19 | -0.14 ± 0.06 | -0.14 ± 0.15 |
| | | 2 | -0.27 ± 0.63 | -0.77 ± 0.59 | -0.13 ± 0.1 | -0.11 ± 0.2 | -0.17 ± 0.48 |
| | | 3 | -0.31 ± 0.6 | -0.7 ± 0.29 | -0.18 ± 0.19 | -0.16 ± 0.18 | -0.15 ± 0.1 |
| | | 4 | -0.26 ± 0.68 | -0.84 ± 0.3 | -0.14 ± 0.1 | -0.1 ± 0.14 | -0.14 ± 0.08 |
| | | 5 | -0.28 ± 0.48 | -1.02 ± 0.63 | -0.14 ± 0.23 | -0.18 ± 0.51 | -0.17 ± 0.25 |
| | | Mean ± SD | -0.27 ± 0.02 | -0.87 ± 0.12 | -0.15 ± 0.02 | -0.14 ± 0.03 | -0.15 ± 0.01 |
| | | *P* | 0.065 | 0.002 | 0.070 | 0.740 | 0.045 |

Abbreviation: WL, whole lung; ROI-T, ROI-main trachea; ROI-L, ROI-left lobe; ROI-RU, ROI-right upper lobe; ROI-RL, ROI-right lower lobe

**Table S3.** Coefficient of variation (CV) values across all four ROIs

| | $Flow_{in}$ | | | | $Flow_{out}$ | | | |
|---|---|---|---|---|---|---|---|---|
| | ROI-T | ROI-LL | ROI-RU | ROI-RL | ROI-T | ROI-LL | ROI-RU | ROI-RL |
| NS1 | 62.2% | 67.5% | 42.6% | 81.7% | 58.3% | 308.2% | 37.1% | 340.8% |
| NS2 | 62.3% | 59.5% | 45.8% | 71.5% | 65.4% | 188.9% | 42.5% | 148.5% |
| NS3 | 48.5% | 60.0% | 59.6% | 102.8% | 55.7% | 167.6% | 144.3% | 207.5% |
| NS4 | 45.2% | 73.4% | 51.0% | 89.8% | 43.2% | 65.8% | 58.2% | 83.5% |
| NS5 | 52.7% | 52.0% | 46.2% | 69.1% | 51.5% | 73.4% | 172.2% | 197.2% |
| LPS1 | 61.6% | 74.1% | 49.9% | 106.1% | 52.8% | 135.9% | 42.5% | 101.8% |
| LPS2 | 64.9% | 96.5% | 100.8% | 132.7% | 76.1% | 76.7% | 173.1% | 286.4% |
| LPS3 | 43.5% | 68.0% | 72.4% | 63.5% | 41.0% | 106.5% | 114.8% | 63.0% |
| LPS4 | 51.8% | 74.6% | 64.7% | 63.9% | 36.1% | 73.6% | 137.4% | 54.1% |
| LPS5 | 60.7% | 70.5% | 65.2% | 112.8% | 62.2% | 156.6% | 288.2% | 149.3% |

**Table S4.** Power analysis results for the quantitative parameters.

| | **WL** | **ROI-T** | **ROI-LL** | **ROI-RU** | **ROI-RL** |
|---|---|---|---|---|---|
| $T_{arrival}$ | 0.7 | 0.5 | 0.3 | 0.5 | 0.4 |
| $T_{peak}$ | 0.6 | 0.2 | 0.6 | 1.0 | 1.0 |
| $Flow_{in}$ | 1.2 | 0.8 | 2.0 | 2.4 | 3.3 |
| $Flow_{out}$ | 2.7 | 4.1 | 2.2 | 1.1 | 2.4 |

**Table S5.** Normal test results for data distribution

| ROI | Group | $T_{arrival}$ | $T_{peak}$ | $Flow_{in}$ | $Flow_{out}$ |
|---|---|---|---|---|---|
| WL | Control | .972 | .900 | .117 | .875 |
| | LPS | .931 | .888 | .263 | .554 |
| ROI-T | Control | .980 | .878 | .096 | .990 |
| | LPS | .862 | .938 | .014 | .485 |
| ROI-LL | Control | .871 | .885 | .073 | .054 |
| | LPS | .924 | .912 | .652 | .189 |
| ROI-RU | Control | .761 | .946 | .596 | .419 |
| | LPS | .865 | .947 | .692 | .819 |
| ROI-RL | Control | .857 | .988 | .175 | .794 |
| | LPS | .839 | .683 | .416 | .225 |

**Table S6**. Statistical analysis of $T_{arrival}$, $T_{peak}$, $Flow_{in}$ and $Flow_{out}$ parameters

| ROI | $T_{arrival}$ | $T_{peak}$ | $Flow_{in}$ | $Flow_{out}$ |
|---|---|---|---|---|
| WL | .370 [a] | .419 [a] | .124 [a] | .013 [a] |
| ROI-T | .461 [a] | .745 [a] | .095[b] | <.001 [a] |
| ROI-LL | .711 [a] | .418 [a] | .023 [a] | .014 [a] |
| ROI-RU | .548 [b] | .190 [a] | .009 [a] | .148 [a] |
| ROI-RL | .560 [a] | .179 [a] | .002 [a] | .009 [a] |

[a] *Unpaired two-tailed* t-test; [b] Mann-Whitney U test.

**Table S7.** Summary of statistical test results following Bonferroni correction for multiple comparisons.

| ROI | $T_{arrival}$ | $T_{peak}$ | $Flow_{in}$ | $Flow_{out}$ |
|---|---|---|---|---|
| WL | 1.000 | 1.000 | .620 | .065 |
| ROI-T | 1.000 | 1.000 | .475 | .002 |
| ROI-LL | 1.000 | 1.000 | .115 | .070 |
| ROI-RU | 1.000 | .950 | .045 | .740 |
| ROI-RL | 1.000 | .900 | .010 | .045 |

## References


[1] Virgincar RS, Dahlke J, Robertson SH, et al. A portable ventilator with integrated physiologic monitoring for hyperpolarized $^{129}$Xe MRI in rodents. J Magn Reson 2018;295:63-71.

[2] Zhang H, Xie J, Xiao S, et al. Lung morphometry using hyperpolarized $^{129}$Xe multi-b diffusion MRI with compressed sensing in healthy subjects and patients with COPD. Med Phys 2018;45:3097-3108.

[3] Xiao S, Deng H, Duan C, et al. Considering low-rank, sparse and gas-inflow effects constraints for accelerated pulmonary dynamic hyperpolarized $^{129}$Xe MRI. J Magn Reson 2018;290:29-37.

[4] Zhou Q, Li H, Rao Q, et al. Assessment of pulmonary morphometry using hyperpolarized $^{129}$Xe diffusion-weighted MRI with variable-sampling-ratio compressed sensing patterns. Med Phys 2023;50:867-878.

[5] Zhang M, Li H, Li H, et al. Quantitative evaluation of lung injury caused by $PM_{2.5}$ using hyperpolarized gas magnetic resonance. Magn Reson Med 2020;84:569-578.

[6] Zhong J, Zhang H, Ruan W, et al. Simultaneous assessment of both lung morphometry and gas exchange function within a single breath-hold by hyperpolarized $^{129}$Xe MRI. NMR Biomed 2017;30.

[7] Amzajerdian F, Hamedani H, Baron R, et al. Simultaneous quantification of hyperpolarized xenon‐129 ventilation and gas exchange with multi‐breath xenon‐polarization transfer contrast (XTC) MRI. Magn Reson Med 2023.

[8] Wells WM, Viola P, Atsumi H, et al. Multi-modal volume registration by maximization of mutual information. Med Image Anal 1996;1:35-51.

[9] Besl PJ, McKay ND. A method for registration of 3-D shapes. IEEE Trans Pattern Anal Mach Intell 1992;14:239-256.

[10] Dupuich D, Berthezene Y, Clouet PL, et al. Dynamic $^{3}$He imaging for quantification of regional lung ventilation parameters. Magn Reson Med 2003;50:777-783.

[11] Mosbah K, Cremillieux Y, Adeleine P, et al. Quantitative measurements of regional lung ventilation using helium-3 MRI in a methacholine-induced bronchoconstriction model. J Magn Reson Imaging 2006;24:611-616.

[12] Koumellis P, van Beek EJ, Woodhouse N, et al. Quantitative analysis of regional airways obstruction using dynamic hyperpolarized $^{3}$He MRI-preliminary results in children with cystic fibrosis. J Magn Reson Imaging 2005;22:420-426.